Thermo Mechanical Behavior of Nanostructured Plasma Sprayed Zirconia Coatings

Soltani, R.; Garcia, E.; Coyle, T.; Lima, R. S; Marple, B. R.; Moreau, C.

Publisher's version / la version de l'éditeur:
Journal of Thermal Spray Technology, 15, 4, pp. 657-662, 2006

Web page / page Web
http://dx.doi.org/10.1361/105996306X147171
http://nparc.cisti-icist.nrc-cnrc.gc.ca/npsi/ctrl?action=rtdoc&an=15877987&lang=en
http://nparc.cisti-icist.nrc-cnrc.gc.ca/npsi/ctrl?action=rtdoc&an=15877987&lang=fr

Thermo Mechanical Behavior of Nanostructured Plasma Sprayed Zirconia Coatings

R. Soltani, E. Garcia, T. Coyle
Centre for Advanced Coating Technologies, University of Toronto, Ontario, Canada

R.S. Lima, B.R. Marple, C. Moreau
National Research Council Canada, Boucherville, Québec, Canada

Abstract

Retaining non-melted nano-particles of zirconia in the nanostructured coatings has been a challenge in the past. Recently an air plasma spray process was developed to produce coatings which retain more than 30-35% by volume non-melted particles, resulting in a unique structure. The creep/sintering behavior of such thermal barrier coatings deposited from nanostructured feedstock has been measured and compared with deposits produced from hollow sphere powder (HOSP^{TM}). Both feedstocks contain 6-8wt% Y_2O_3 as stabilizer. Flexure and compression creep testing were conducted under several different loads and temperatures to obtain creep exponents and parameters.

Introduction

Plasma sprayed thermal barrier coatings for different applications are still being developed, however, there is not much information on high temperature properties of these new coatings. Operating temperatures for zirconia coatings are usually around/above 1000°C. The presence of relatively high compressive stresses at the coating surface lead to stress relaxation by creep and/or sintering. Shrinkage at high temperatures followed by crack initiation and propagation during cooling will cause spallation of the coating and consequently shorten the life time of the deposit.

Creep/sintering behaviour of zirconia and its plasma sprayed form have been investigated by several researchers [1-10]. Elastic modulus, hardness and even thermal conductivity vary with temperature, and so affect the residual stresses present at the operating temperature [1, 11]. Sintering at service temperatures may heal micro cracks and eliminate some porosity, creating a denser structure which could be an advantage in reducing oxygen transport to the bond coat and reducing its oxidation but unfortunately upon cooling micro cracks reappear again. Eventually the coating becomes sufficiently damaged that spalling occurs. The thickness of the coating is another important factor; nowadays depositions of more than 1 mm in thickness are demanded to increase protection and reduce heat transfer. The thicker the coating, the greater the thermal gradients present during service, which results in higher stresses within the cross section of material [3].

Therefore investigating high temperature properties of thermal barrier coatings is a priority to developing a new top coat structure. Bimodal structured thermal barrier coatings can provide the improved performance of an alternative material without the necessity of redesigning the entire component. There are several methods to produce nanostructured coatings, including thermal spray processes. Researchers have shown that nanostructured coatings can exhibit better properties than conventional coatings of the same composition [12-18].

In the current work, partially stabilized zirconia (PSZ) coatings were deposited by air plasma spraying. Two different types of powder feed stock were employed, a conventional micron particle size powder and a nanostructured particle powder. The influence of the powder type on the thermomechanical behaviour of the coatings was investigated.

Experimental Pprocedure

Two commercially available 6-8 wt% Y_2O_3-PSZ powders were used to deposit coatings by air plasma spraying. 204B-NS (Sulzer-Metco, NY, USA) with a SG-100 (Praxair, Concord, NH, USA) plasma torch and Nanox coatings were sprayed using the F4-MB (Sulzer-Metco, NY, USA) torch. The nano structured powder was Nanox S4007 (Inframat Corp., CT, USA). This powder consisted of agglomerated

particles 15-150 μm in diameter made up of crystallites on the order of 200 nm. The micron size powder was Metco 204B-NS (hollow oven spherical particles, HOSP^{TM}) from Sulzer Metco, with a particle size of 45-75 μm, Fig.1.

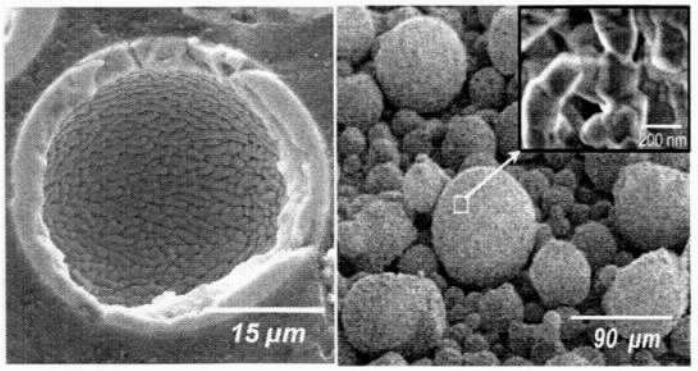

Figure 1: Typical SEM image of 204B-NS feedstock particle, left; and Nanox S4007,right.

Substrates were carbon steel plates, 4 mm thick with dimensions of 50x50x4 mm (WxLxH) . Before coating surface of the substrates was alumina grit blasted to a rms roughness of approximately 4 μm as measured using a Surfometer (Precision Devices Inc., MI, USA) The thickness of the coating was more than 3 mm. Samples then were cut to 3x4x40 mm (HxWxL). The substrates were detached by cutting down the thickness of the carbon plates with a precision cutter to 1 mm. Since no bond coat was applied and residual stresses were high because of large thickness, the coatings could be easily separated from the substrate.

The powder and coating microstructures were examined by scanning electron microscopy (SEM, Hitachi S-4500, Tokyo, Japan) using low voltage electron microscopy method. An image analyzer (Clemex Vision Professional software, QC, Canada) was used to measure the average porosity of each sample and the non melted nano particle areas for the nanostructured deposit. The pore size and distribution in samples were measured with a mercury intrusion porosimeter (MIP, Auto Pore III, Micromeritics Instrument Corp., GA, USA). The chemical composition of the powders was obtained with flame photometry (FP) and inductively coupled plasma (ICP). Creep tests were conducted employing four-point bend and compression tests. Details have been presented elsewhere [19].

Results and Discussion

Characterization

Prior to conducting creep tests, SEM images of the conventional and nanostructured coatings deposited using 204B-NS and Nanox powders were taken, Figs. 2 and 3. The nanostructured sample had a unique arrangement of non molten nano particles in a significant volume of the sample. Fig. 3 clearly shows that there is a significant presence of non-molten nano YSZ feedstock particles embedded in the coating microstructure. The melting process in plasma stream will be accelerated by geometry of 204B-NS particle types. The thin shell of this feedstock increases the probability of having fully melted particles which results in a high flattening ratio and very thin final splats in the coating. Zirconia is a thermal barrier because of low conductivity, therefore heat transfer to the core of solid particle would not be fast and may lead to a semi melted/ unmelted one.

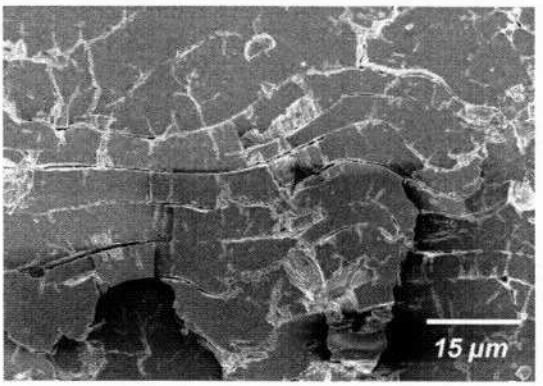

Figure 2: SEM image of a polished surface of 204B-NS deposit showing layers of splats.

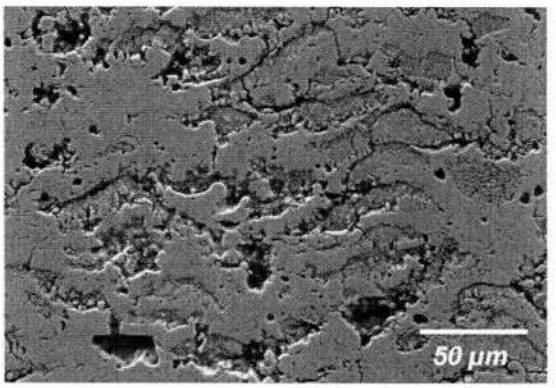

Figure 3: SEM image of a polished surface of nanostructured deposit revealing melted and unmelted areas.

Porosity and non-molten nano particle areas in deposits were investigated by image analysis; (Table 1). From each sample twenty images were taken. Results showed that porosity of nanostructured sample was more than twice of that in 204B-NS coating and non molten nano particles occupied a large area of approximately 30-35%. It should be mentioned that image analysis results are strongly dependent on resolution and contrast of different features on images and this contrast is not enough to differentiate nano porosities among non melted nano particles in low magnifications. Therefore it is likely that the porosity results understimate the level of porosity actually present in the coating.

Table 1: Porosity and nano area percentages of nanostructured and 204B-NS coatings.

Coating	*Porosity (%)*	*Nano (%)*	*Density (gr/cm^3)*
204B-NS	*11 ± 1*	*0*	*5.07*
Nanox	*>25 ± 2*	*30-35*	*4.11*

In order to information on the pore size and distribution in samples, mercury intrusion porosimetry tests were conducted and results showed that there was a wider range of pore sizes in the nanostructured coating and that this coating had more porosity (a larger amount of mercury intrusion), Fig. 4.

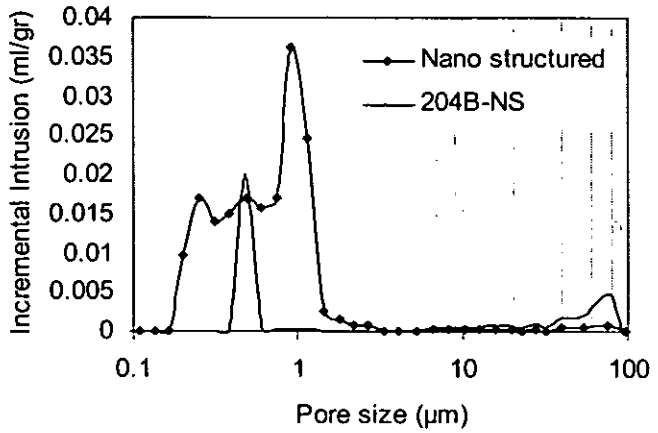

Figure 4: Mercury porosimetry of nanostructured and 204B-NS coatings showing higher porosity and a wider pore size range for nanostructured deposit.

Compositional analysis was performed to investigate the levels of different species present in the two feedstocks and did not indicate any major differences between the two materials, (Table 2). Particular components such as silica, alumina and titania which may create a glassy phase at grain boundaries, were peresent in almost the same amounts in both powders therefore, if these constituents have any effect on the creep/sintering properties of samples, it is expected that it would similar for both. Therefore a comparison based on structural considerations should be valid.

Creep

Creep tests on 204B-NS free-standing deposits were conducted employing a SiC four-point flexure fixture under a range of stresses and temperatures to obtain creep exponents and activation energy values of the coating, Figs. 5 and 6. These samples were strong enough to withstand loads up to almost 50 N in this test method. Samples show a high strain rate in the primary phase and by increasing strain, creep rate is reduced dramatically, approaching a steady state rate. By raising stress level, at constant temperature (1000°C), creep strain shows an increase too but creep rate at secondary phase does not change significantly. This indicates a low dependency on stress, Fig. 5.

Table 2: Chemical composition of two feedstocsk; nanostructured and 204B-NS.

	Nanox (%)	204B-NS (%)	Technique
Al_2O_3	0,66	0,66	ICP
CuO	0,007	0,008	ICP
CaO	0,025	0,026	ICP
Fe_2O_3	0,006	0,009	ICP
HfO_2	1,74	1,52	ICP
P_2O_5	0,04	0,04	ICP
SiO_2	0,12	0,11	ICP
TiO_2	0,06	0,14	ICP
Y_2O_3	6,43	7,30	ICP
Na_2O	0,03	0,02	FP

Figure 6 shows creep strain of the same samples at a range of temperatures. Similar behavior is obtained in changing creep rate at different temperature levels, but a higher dependency on temperature than stress is observed. This is probably indicating a change in the dominant creep mechanism.

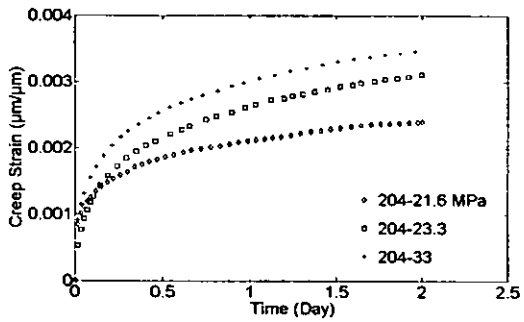

Figure 5: Creep strain of 204B-NS sample under different stress levels at 1000°C for 2 days.

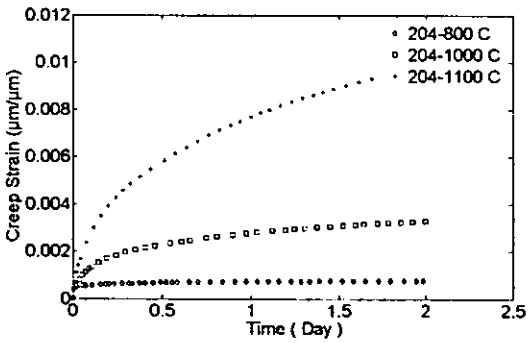

Figure 6: Creep strain of 204B-NS samples under 24 MPa for 2 days at different temperatures.

Since nanostructured samples could not resist even very low loads in flexure, a compression technique was used to measure creep properties of these deposits. Based on previous

experiments, these two methods showed an acceptable consistency in results. Nutt and Lipetzky found the same reliablility for alumina reinforced with SiC whiskers [20].

Figures 7 and 8 show creep strain of nanostructured coatings under a range of stresses and temperatures for two days, respectively. As is clear, this nanostructured coating exhibits a significantly higher creep strain than the 204B-NS deposits.

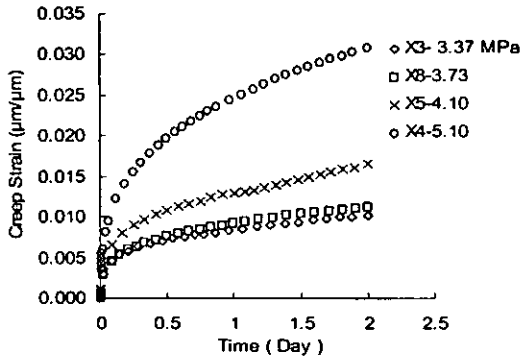

Figure 7: Compression creep strain of nanostructured samples under different stresses at 1000 °C

Like the creep behaviour of 204B-NS samples, nanostructured deposits show a primary and secondary creep. As load and temperature of the test conditions are increased, the amount of creep strain rises too but this dependency is stronger on temperature, as is clear from Fig. 8.

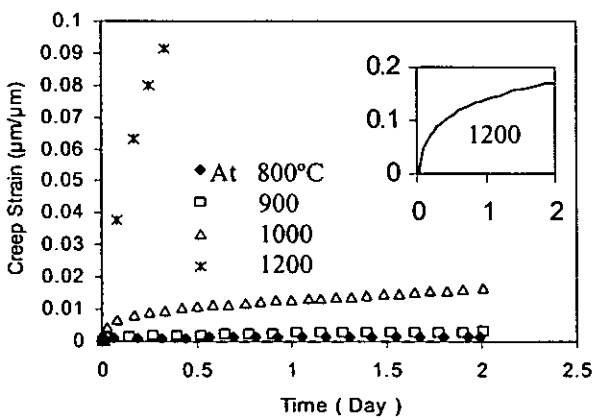

Figure 8: Creep strain of Nano structured samples at different temperatures under ~4 MPa compressive stress.

By obtaining creep data and using power-law creep and Arrhenius equations, stress exponents and activation energies of the coatings were calculated, Figs. 9 and 10. These outcomes are consistent with creep strain results. The nanostructured deposit shows a lower activation energy of 165 KJ/mol compared to 192 KJ/mol for the 204B-NS sample, which indicates a higher creep strain under the same conditions. In addition, calculation of stress exponent of nanostructured specimens indicates a higher value (n ~ 2) for this sample compared to its counterpart (n ~ 1). This difference in creep exponents may be an indication of changing creep mechanisms in samples. To investigate the dominant mechanisms in each sample an extensive SEM work was done and some of these images are shown in Figs.11-13.

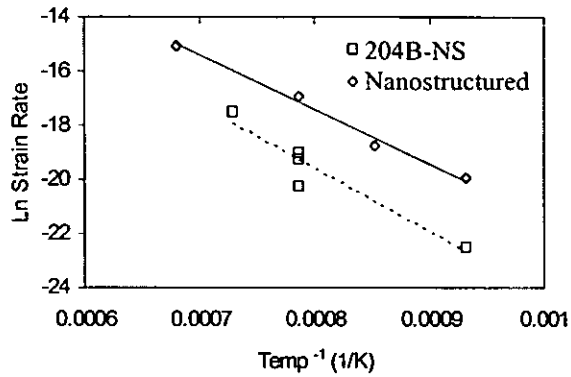

Figure 9: Activation energy of nanostructured and 204B-NS samples, 165 and 192 KJ/mol, respectively.

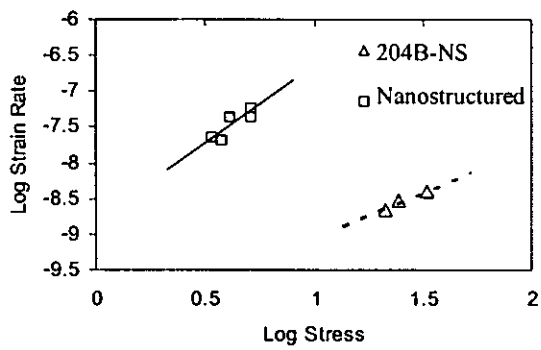

Figure 10: Stress exponents of 204B-NS and nanostructured samples; 1.3 and 2.2 , respectively.

In 204B-NS fractured coating after creep, three different mechanisms of sintering proposed by T.W.Clyne are observed [12]: intra-splat and inter-splat grain growth and micro crack healing. Surface diffusion result in grooving, touching and necking of columnar grains at micro cracks edges and consequently closing them. The same process happens for growth of columnar grains. In this structure splat sliding which may help healing of huge network of micro cracks as well, looks to be the dominant mechanism of creep in direction parallel to splat faces. The SEM images in Fig. 11 show intra (a) and inter (c) splat grain growth, and micro crack healing (b).

More SEM and TEM image analyses are being carried out to investigate effects of trace materials as a viscous phase at grain boundaries.

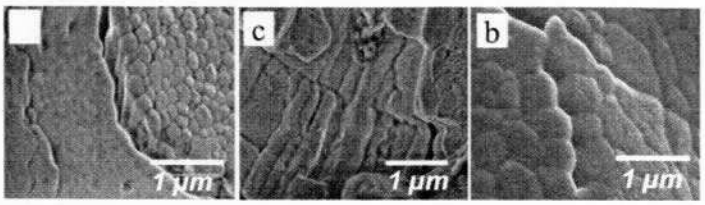

Figure 11: After creep SEM images of 204B-NS (two days at 1000 °C under 21 MPa);(a) intra-splat grain growth, (b) micro crack healing and (c) inter-splat grain growth.

The nanostructured sample has a different array of splats and non molten nano particles, Figs. 12 and 13. The structure appears to consist of one or two successive layers of conventional splats and then a deposit of nano particles. SEM investigation showed that micro-crack healing still occured in this structure however, because of very low volume fraction of micro cracks in the structure, the contribution from this source could not be as large as in the 204B-NS coatings. In nanostructured sample, columnar grain growth was observed too however, very few locations in the structure could be found to have a pile up of conventional splats. As it is clear porosity of nanostructured sample is much more than 204B-NS. Usually this means a higher free surface available for diffusion of anion and cations which consequently increases creep rate too.

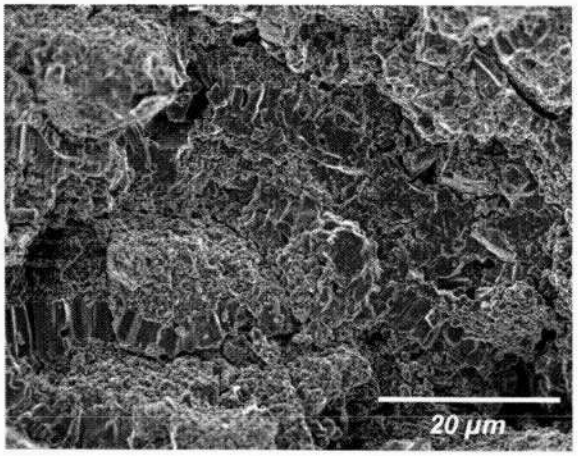

Figure 12: After creep SEM image of fractured nanostructured coating (2 days at 1000°C under 5.1 MPa).

Based on SEM examination, grain boundary sliding and rearrangement of nano particles seem to be the dominant mechanisms and responsible for the high creep strain of nanostructured coating. As is clear in Fig. 13, non-molten nano particles were still present even after creep test and a huge amount of nano porosity still remained among these particles, making diffusion of species much faster and easier.

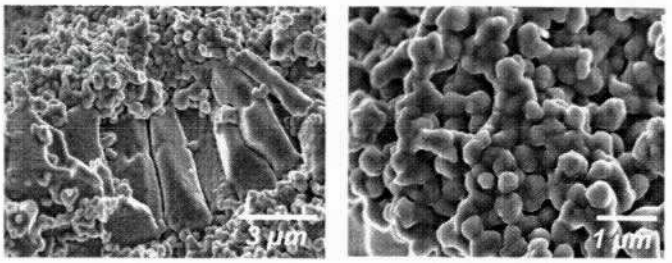

Figure 13: SEM images of nanostructured deposit at higher magnifications.

Conclusion

Nanostructured zirconia thermal barrier coatings were successfully deposited with more than 30% preserved non molten nano particles in the coating. Creep properties of this structure were measured and compared with a conventional coating. Results showed a higher creep strain for the nanostructured sample than for the conventional, activation energies of 165 and 192 KJ/mol and stress exponent of 2.2 and 1.3 for the nanostructured and conventional deposits, respectively. The dominant creep mechanism for 204B-NS coating was believed to be splat sliding along with micro crack healing by means of grain boundary and surface diffusion. Having higher creep rate in nanostructured sample causes higher stress relaxation in elevated temperatures as well, but when the coating cools down then a tensile stress is introduced into the coating, cracks will tend to reappear and the coating may spall off after a sequence of thermal cycles. However, nanostructured ceramic coatings are known for exhibiting higher toughness and higher bond strength values when compared to those of the conventional coatings [21-22]. In addition to that, the porous non-molten nano particles embedded in the coating microstructure probably exhibit very low elastic modulus values, i.e., they may act as compliance or yielding regions to stress. Therefore, these nano YSZ coatings may withstand the stresses generated on cooling, which would provide an optimized TBC. Thermal cycle tests are pending to verify if nano TBCs exhibit improved performance when compared to conventional ones.

References

1. D. Zhu and R.A Miller, Determination of Creep Behavior of Thermal Barrier Coatings under Laser Imposed Temperature and Stress Gradients, *NASA Technical Memorandum 113169*, ARL-TR-1556, 1997
2. D. Zhu and R.A Miller, Sintering and Creep Behavior of Plasma-Sprayed Zirconia and Hafnia-Based Thermal Barrier Coatings, J. Surf. Coat. Technol., Vol 108-109, 1998, p 114-120
3. E.F. RFejda, D.F. Socie and T. Itoh, Deformation Behavior of Plasma-Sprayed Thick Thermal Barrier Coatings,, Vol 113, 1999, p 218-226

4. A.H. Chokshi, Diffusion Creep in Oxide Ceramics , J. The European Ceramic Society, Vol 22, 2002, p 2469-2478
5. A.H. Chokshi, Diffusion, Diffusion Creep and Grain Growth Characteristics of Nanocrystalline and Fine-Grained Monoclinic, Tetragonal and Cubic Zirconia, Scripta Materialia, Vol 48, 2003, p 791-796
6. R. Schaller, M. Daraktciev, Mechanical Spectroscopy of Creep Appearance in Fine-Grained Yttria-Stabilized Zirconia ; J. The European Ceramic Society, Vol 22, 2002, p. 2461-2467
7. M.J. Adnrews, M.K. Ferber and E. Lara-Curzio, Mechanical Properties of Zirconia–Based Ceramics as Functions of Temperature, J. The European Ceramic Society, Vol 22, 2002, p. 2633-2639
8. K. Kokini, Y.R. Takeuchi and B.D. Choules, Surface Thermal Cracking of Thermal Barrier Coatings Owing to Stress Relaxation: Zirconia vs. Mullite, J. Surf. Coat. Technol., VoL 82, 1996, p. 77-82
9. L. Vasylkiv, Y. Skka, and V.V.Skorokhod, Low-Temperature Processing and Mechanical Properties of Zirconia and Zirconia-Alumina Nanoceramics, J. Am. Ceram. Soc., Vol 86 (No. 2),2003, p.299-304
10. M. Daraktchiev and R. Schaller, High-Temperature Mechanical Loss Behavior of 3 mol% yttria-stabilized Tetragonal Zirconia Polycrystals ,3Y-TZP), J. Phys. Stat. Sol. Vol 2, 2003, p. 293-304
11. R.S. Lima, a. Kucuk and C.C. Berndt, Bimodal Distribution of Mechanical Properties in Plasma Sprayed Nanostructured Partially Stabilized Zirconia, J. Mater. Sci. Eng. A, Vol 327, 2002, p. 224-232
12. J.A. Thompson, T.W. Clyne, The Effect of Top Coat Sintering on Ceramic Spallation in Plasma Sprayed Thermal Barrier Coatings, The 13th International Conference on Surface Modification Technology (SMT XIII), Convention City, Singapore, 1999, p. 177-182
13. L. Shaw, D. Goerman, R. Ren, and M. Gell, The Dependency of Microstructure and Properties of Nanostructured Coatings on Plasma Spray Conditions, J. Surf. Coat. Technol., Vol 130, 2000, p. 1-8
14. M. Gell, E.H. Jordan, Y.H. Sohn and D. Gberman, Development and Implementation of Plasma Sprayed Nanostructured Ceramic Coatings, J. Surf. Coat. Technol., Vol 146-147, 2001, p. 48-54
15. H. Chen and C.X. Ding, Nanostructured Zirconia Coating Prepared by Atmospheric Plasma Spraying, , J. Surf. Coat. Technol., Vol 150, 2002, p. 31-36
16. H. Chen and C.X. Ding, Microstructural Characterization of Plasma Sprayed Nanostructured Zirconia Powders and Coatings ; J. European Ceramic Society, Vol 23, 2003, p. 491-497
17. M. Gell, L. Shaw, Fabrication and Evaluation of Plasma Sprayed Nanostructured Alumina-Titania Coatings with Superior Properties, J. Mater. Sci. Eng. A, Vol 301, 2001, p. 80-89
18. R.S. Lima, C.C. Berndt, Evaluation of Microhardness and Elastic Modulus of Thermally Sprayed Nanostructured Zirconia Coatings, J. Surf. Coat. Technol., Vol 135, 2001, p. 166-172
19. R. Soltani, T.W. Coyle, J. Mostaghimi, Thermo-Physical Property of Bimodal Structured Plasma Sprayed TBCs, To be published.
20. S.R. Nutt and P.L. Lipetzky, Creep Deformation of Alumina-SiC Composites, J. Mater. Sci. Eng. A, Vol 126, 1990, p. 165-172
21. P. Bansal, N. Padture, A. Vasiliev, Improved Interfacial Mechanical Properties of Al_2O_3-13TiO_2 Plasma-Sprayed Coatings Derived from Nanocrystalline Powders, Acta Materialia, Vol 51, 2003, p 2959-2970
22. H. Luo, D. Goberman, L. Shaw, M. Gell, Indentation Fracture Behavior of Plasma-Sprayed Nanostructured Al_2O_3-13wt%TiO_2 Coatings, Mater. Sci. and Eng. A, Vol 346, 2003, p 237-245